Letter | Editors' Suggestion

Anomalous Near-Field Heat Transfer in Carbon-Based Nanostructures with Edge States

Gaomin Tang,[1,*] Han Hoe Yap,[2,1,†] Jie Ren,[3,‡] and Jian-Sheng Wang[1,§]

[1] *Department of Physics, National University of Singapore, Singapore 117551, Republic of Singapore*
[2] *NUS Graduate School for Integrative Sciences and Engineering, Singapore 117456, Republic of Singapore*
[3] *Center for Phononics and Thermal Energy Science, China-EU Joint Center for Nanophononics, Shanghai Key Laboratory of Special Artificial Microstructure Materials and Technology, School of Physics Science and Engineering, Tongji University, Shanghai 200092 China*

(Received 2 October 2018; revised manuscript received 14 February 2019; published 26 March 2019)

We find an unusually optimal near-field heat transfer, where the maximum heat transfer is reached at experimentally feasible gap separation. We attribute this to the localized zero-energy electronic edge states, which also substantially change the near-field behaviors. We demonstrate these anomalous behaviors in two typical carbon-based nanostructures: zigzag single-walled carbon nanotubes and graphene nanotriangles. For the system of carbon nanotubes, the maximal heat flux in this work surpasses all the previous results reported so far. The underlying mechanism for the peculiar effects is uncovered from a simple Su-Schrieffer-Heeger model. Our findings also offer a route to achieve an active near-field thermal switch, where the heat flux can be modulated through tuning the presence or absence of edge states.

DOI: 10.1103/PhysRevApplied.11.031004

Introduction.– Far-field heat transfer can be well described by Planck's theory of blackbody radiation [1] and obeys the Stefan-Boltzmann law. When the gap separation between two bodies becomes smaller than Wien's wavelength, heat transfer in the near field becomes distance dependent and is much larger than that in the far field [2–4]. Within the fluctuational electrodynamics [3–5], the near-field heat flux typically increases as the two bodies become closer. As such, great efforts have been dedicated to reducing the gap sizes from orders of 1 μm [6–8] to a few nanometers [9–12], resulting in several folds to several orders of heat-transfer enhancement compared to the corresponding far-field results.

Besides, by reducing gap distance, several other approaches have been brought forward to enhance near-field heat transfer. Pendry showed that the heat flux can be greatly enhanced by tuning the resistivity of the material [13]. Covering both surfaces with adsorbates, so that resonant photon tunneling happens between adsorbate vibrational modes, can also enhance the heat flux [14]. Two types of surface waves have been mainly used to increase heat transfer in the near field. One is surface phonon polariton supported in polar dielectrics, such as SiC and SiO_2 [15–18]. The other type is surface plasmon polariton on materials supporting low-frequency plasmon [14,17–20], such as graphene [21–23], black phosphorus [24], and silicon [25,26]. Through the shuttling effect, a supplementary flux superimposes to the one produced by the mean gradient and enhances heat exchange [27]. Using hyperbolic metamaterials can help to enhance heat transfer as well [28–30]. Theoretically, recent works attribute the origin of heat-transfer enhancement between nanoparticles to a full coupling between all multipolar modes [31,32].

In this letter, we report peculiar vacuum-gap dependence and enhancement of near-field heat transfer in the presence of electronic edge states. We employ the nonequilibrium Green's function (NEGF) formalism within the random phase approximation (RPA). The peculiar behaviors are demonstrated using zigzag single-walled carbon nanotubes (SWCNTs) [See Fig. 1(a)] and graphene nanotriangles forming a bowtie shape [Fig. 1(b)]. For heat transfer between carbon nanotubes, the maximal heat flux is significantly large. We uncover the mechanism using the simple Su-Schrieffer-Heeger (SSH) chains.

Theoretical formalism.– When two metallic surfaces are separated by a vacuum gap, which is much smaller than Wien's wavelength λ_{th} (several micrometers at room temperature), the contribution to heat transfer from the retarded vector potential can be ignored, and the electron-electron interaction dominates the heat transfer [23,33–38]. If the vacuum gap is below around 1.5 nm, electron tunneling can happen [35,39], the picture dominated by

*gaomin.tang@unibas.ch
†e0095832@u.nus.edu
‡xonics@tongji.edu.cn
§phywjs@nus.edu.sg

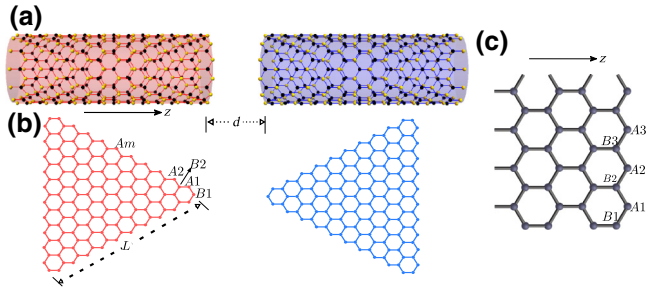

FIG. 1. Near-field heat transfer between (a) two SWCNTs and (b) graphene nanotriangles, which are separated by a vacuum gap with distance d. (c) Lattice structure of a zigzag SWCNT corresponding to the left side in (a). For the graphene nanotriangles shown, they are equilateral with the side length $L = 4.26$ nm.

electron-electron interaction does not apply. So our formalism below can faithfully describe heat transfer with the vacuum gap d in the range 1.5 nm $< d \ll \lambda_{\rm th}$. The lattice Hamiltonian of a general electron-electron interaction mediated heat transfer reads as follows:

$$H = \sum_{mn} c_m^\dagger h_{mn} c_n + \frac{e_0^2}{2} \sum_{mn} c_m^\dagger c_m v_{mn} c_n^\dagger c_n, \tag{1}$$

with e_0 the elementary charge. c_m ($c_m^\dagger$) is the fermionic annihilation (creation) operator of lattice site m, and h_{mn} is the on-site energy for $m = n$ and hopping parameter for $m \neq n$ locating on the same side. For the situation of indices m and n locating on different sides, h_{mn} vanishes, and this implies that electron tunneling from one side to the other is impossible. v_{mn} is the Coulomb potential between sites m and n. Heat transfer occurs via the charge fluctuations between the electronic states sitting at the edges from both sides.

Under RPA, the charge polarization $\Pi^r_{mn}(\omega)$ is given by [40]

$$\Pi^r_{mn}(\omega) = e_0^2 \int \frac{dE}{2\pi} \mathcal{A}_{mn}(E) f(E) \Big[G^r_{mn}(E_+) + G^a_{nm}(E_-) \Big], \tag{2}$$

with $E_\pm = E \pm \hbar\omega$ and $f(E)$ the Fermi distribution function in the corresponding side. The retarded (advanced) Green's functions $G^{r(a)}$ are obtained from the noninteracting part of the Hamiltonian, and $\mathcal{A}(E) = -2\mathrm{Im}[G^r(E)]$ is the electronic spectral function. A damping constant η is included in calculating Green's function to account for possible dissipations due to the electron-phonon interaction and impurity scattering under the relaxation-time approxmation [41]. The charge susceptibility $\chi_\alpha(\omega)$ is expressed as

$$\chi_\alpha(\omega) = \Pi^r_\alpha(\omega)[\mathbf{I} - v_\alpha \Pi^r_\alpha(\omega)]^{-1}, \tag{3}$$

with the identity matrix $\mathbf{I}$, intraside Coulomb interaction v_α, and $\alpha = L, R$. The heat current reads as follows [23,36]:

$$J = \int_0^\infty \frac{d\omega}{2\pi} \hbar\omega \mathcal{T}(\omega) \Big[N_L(\omega) - N_R(\omega) \Big], \tag{4}$$

with $N_\alpha(\omega) = 1/[e^{\hbar\omega/(k_B T_\alpha)} - 1]$ the Bose-Einstein distribution. The spectral transfer function is

$$\mathcal{T}(\omega) = 4\mathrm{Tr}\Big\{ \Delta^\dagger(\omega) v_{RL} \mathrm{Im}[\chi_L(\omega)] v_{LR} \Delta(\omega) \mathrm{Im}[\chi_R(\omega)] \Big\}, \tag{5}$$

where the trace is over lattice sites, and

$$\Delta(\omega) = [\mathbf{I} - \chi_R(\omega) v_{RL} \chi_L(\omega) v_{LR}]^{-1}. \tag{6}$$

The entries of the Coulomb matrices between left and right sides are $v_{mn} = 1/(4\pi\epsilon_0 d_{mn})$ with ϵ_0 the vacuum dielectric constant and d_{mn} the distance between site m and n. The formalism based on NEGF has been shown [23,35,36] to reduce to that by the fluctuational electrodynamics [3–5] in the nonretardation limit and be equivalent to that given by Mahan [33].

For calculating zigzag SWCNTs and graphene nanotriangles, we consider the spin degenerate case, so that $\Pi^r_{mn}(\omega)$ obtained from Eq. (2) should be multiplied by 2 to take both spins into account. The intraside Coulomb interaction is $v_{mn} = 1/(4\pi\epsilon_0\varepsilon d_{mn})$ for $m \neq n$ with ε describing the effect of the background dielectric medium. A self-interaction of 0.58 a.u. is included for $m = n$ [41]. Temperatures of the left and right sides are set as $T_L = 400$ K and $T_R = 300$ K, respectively.

Heat transfer between zigzag SWCNTs.– It has been reported that zero-energy localized states (Fujita's edge states) emerge at the edges of zigzag SWCNTs [42–44]. The contribution of heat transfer between two bodies are mainly from the surface atoms, which are denoted as *Am* and *Bm* with index m as shown in Fig. 1(c). The local electronic density of states for the atoms *Am* are sharply peaked at zero energy as shown in Fig. S1(a) of the Supplemental Material [38]. We use M to denote the total number of *Am* sites. Due to the $O(2)$ rotational invariance of carbon nanotubes, all the atoms of *Am* and *Bm* are geometrically equivalent in their respective sides. The carbon-carbon bond length is 1.42 Å, and the nearest-neighbor hopping constant is 2.5 eV. The recursive Green's function technique [45] is used in getting Green's function of the surface sites with the damping constant $\eta = 25$ meV.

In Fig. 2(a), we plot heat currents versus gap distances with different radii. The nonmonotonic behavior is found for the cases of $M = 15$, 20, and 25 shown in Fig. 2(a). The maximal heat currents are almost identical for these three cases. We find that the larger the nanotube radii, the longer the distances for achieving corresponding maximal

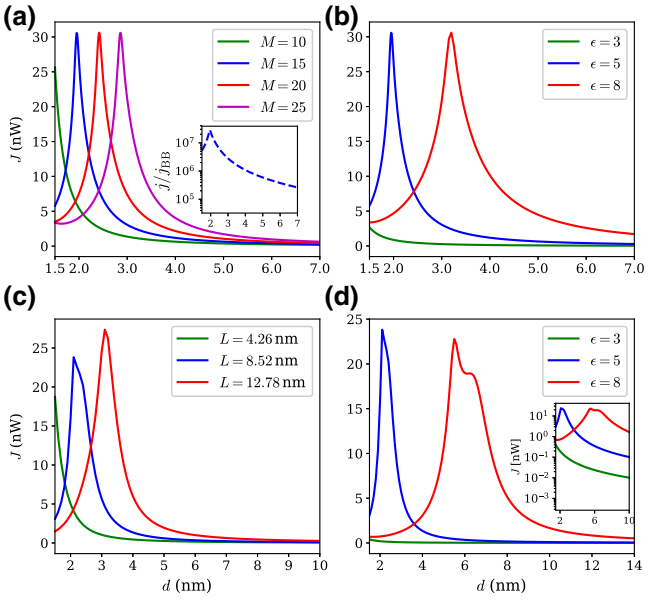

FIG. 2. Gap-separation dependences of heat current between zigzag SWCNTs for different M with $\varepsilon = 5$ (a), and for different ε with $M = 15$ (b). Gap-separation dependences of heat current between graphene nanotriangles for different L with $\varepsilon = 5$ (c), and for different ε with $L = 8.52$ nm (d).

heat current. The condition(s), under which the heat current reaches maximum with several nanometers of gap separation for zigzag SWCNTs, can be obtained analytically [38]. The critical distance is approximately the summation of all entries of the real parts of the charge susceptibility at zero frequency, that is,

$$d_c \approx -\frac{1}{4\pi\epsilon_0}\sum_{m,n}\mathrm{Re}[\chi_{mn}(\omega=0)]. \tag{7}$$

Since the terminal sites contribute the critical distance in an additive way, a small amount of disorder or vacancies only decrease the critical distance slightly without changing the maximal heat current. For the case of $M = 10$ in Fig. 2(a), the critical distance appears below 1.5 nm as predicted by Eq. (7). For such an extremely short distance, heat transfer may have a contribution from electron tunneling [35,39], which is not included in our model.

Gap-separation dependence of heat current for different dielectric constants ε is shown in Fig. 2(b). One can find that the critical distance disappears for the case with $\varepsilon \leq 3$. With increasing dielectric constant ε, the critical distance shifts to larger values. This is because the amplitudes of the real parts of charge susceptibility at zero frequency increase as a consequence of less screening. Different dielectric constants can be realized by encapsulating the carbon nanotubes with different dielectric materials. Inserting a dielectric material as a core of the nanotubes can change the dielectric constant as well.

The area formed by a zigzag SWCNT with $M = 15$ is 1.1 nm^2, so that the corresponding heat flux j, i.e., heat current per area, is about 2.8×10^{10} W/m^2 with maximal heat current $J = 30.6$ nW at critical distance. This heat flux is several orders of magnitude larger than those mediated by surface phonon polaritons or surface plasmon polaritons [26], and almost comparable to that of heat conduction. In the inset of Fig. 2(a), we plot the ratio between the heat flux corresponding to $M = 15$ and the blackbody limit $j_{\mathrm{BB}} = 9.9 \times 10^2$ W/m^2. The maximal heat flux j is about 7 orders of magnitude larger than j_{BB}. To compare heat transfer with the systems without edge states, we calculate the heat current between armchair SWCNTs, which do not host zero-energy localized states. The result is shown in Fig. S2 of the Supplemental Material [38]. We find that the heat current in systems with armchair SWCNTs is much smaller than that of with zigzag SWCNTs. Since the structure-controlled growth of SWCNTs is rapidly advanced [46,47], the results shown can be experimentally realized in the near future.

Heat transfer between graphene nanotriangles.– We further show the nonmonotonic behavior of gap separation for heat transfer between two equilateral graphene nanotriangles. We focus on the vertex-to-vertex geometry forming a bowtie shape as shown in Fig. 1(b), and side length is L. The nearest-neighbor hopping constant is chosen as 2.8 eV, and the damping constant $\eta = 25$ meV. The electronic Green's function is calculated recursively [48]. The graphene nanotriangles can be maintained at thermal equilibrium through optical pumping or by being attached to additional electrodes. As shown in Fig. S2 of the Supplemental Material [38], the main contributions to the heat transfer are from sites Am as indicated in Fig. 1(b), which have strongly localized zero-energy states. Gap-separation dependences of heat current by varying side length L and dielectric constant ε are shown Figs. 2(c) and 2(d), respectively. Similarly to the behaviors found in Fig. 2(a) for zigzag SWCNTs, we observe nonmonotonic behavior for $L = 8.52$ nm, and $L = 12.78$ nm as shown in Fig. 2(c). From Fig. 2(d), we see that increasing the dielectric constant in graphene nanotriangles increases the critical distance as well, which is as shown in Fig. 2(b).

Heat transfer between SSH chains.– We bring forth a theoretical understanding for the peculiar phenomenon observed using one-dimensional SSH chains, which undergo topological phase transitions by varying the hopping parameters [49]. The Hamiltonian of a SSH chain for side α reads as follows:

$$H_{0\alpha} = -(1+\lambda_\alpha)t\sum_{n=1}^{N}(c_{An}^\dagger c_{Bn} + \mathrm{H.c.}) - (1-\lambda_\alpha)t\sum_{n=1}^{N-1}(c_{An+1}^\dagger c_{Bn} + \mathrm{H.c.}), \tag{8}$$

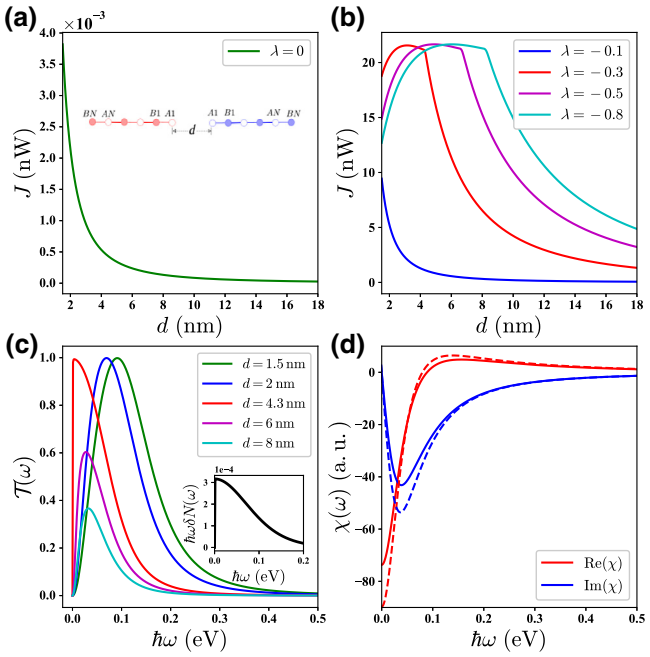

FIG. 3. Gap-separation dependences of heat current in the metallic phase (a) and the topologically nontrivial phase (b). (c) The spectral transfer functions for different gap separations with $\lambda = -0.3$. (d) Real and imaginary parts of the charge susceptibility of the site $A1$ with temperatures 400 K (χ_L, solid lines) and 300 K (χ_R, dashed lines).

with N the number of lattice sites, and $\lambda_\alpha \in [-1, 1]$. We consider the case where heat transfer happens between two end sites, both of which are labeled as $A1$ as shown in the inset of Fig. 3(a). Under this consideration, v_α vanishes, so that $\chi_\alpha(\omega) = \Pi^r_\alpha(\omega)$. We set $\lambda_L = \lambda_R = \lambda$ and the hopping constant $t = 2.2$ eV during the calculation. A damping constant $\eta = 22$ meV is added to each site in calculating electronic Green's function [50]. The energy spectrum of an open SSH chain is shown in the right inset of Fig. 4(a). When $\lambda > 0$, SSH chain is in a trivial insulator state without in-gap state, and it is in a metallic state for $\lambda = 0$ where the gap closes. However, the gap reopens in the topologically nontrivial region with $\lambda < 0$, and zero-energy in-gap states appear.

The gap-separation dependence of heat current in the metallic phase and the topologically nontrivial phase are shown in Figs. 3(a) and 3(b), respectively. For the case of $\lambda = -0.3$, the spectral transfer functions for different gap separations d and the charge susceptibilities $\chi(\omega)$ of the end sites $A1$ are plotted in Figs. 3(c) and 3(d), respectively. There exists a critical gap distance d_c, at which the heat flux achieves its maximum in the presence of edge state. The critical distance is approximately expressed as $d_c \approx -\mathrm{Re}[\chi_L(\omega = 0)]/(4\pi\epsilon_0)$. [For $\lambda = -0.3$, $d_c \approx 4.3$ nm $= 81.26$ a.u. The value in a.u. is between $|\mathrm{Re}[\chi_L(\omega = 0)]|$ and $|\mathrm{Re}[\chi_R(\omega = 0)]|$, which are shown in Fig. 3(d).] The explanation of this peculiar distance dependence is as follows. Near the critical distance d_c, $\mathrm{Re}[\chi_L(\omega \to 0)]v_{LR} \approx \mathrm{Re}[\chi_R(\omega \to 0)]v_{RL} \approx -1$. One also has $\mathrm{Im}[\chi_{L/R}(\omega \to 0)] \approx 0$, so that $v_{LR}\Delta\mathrm{Im}(\chi_R)|_{\omega\to 0} \approx i/2$, hence we have $\mathcal{T}(\omega \to 0) \approx 1$ around the critical distance. Since the function $\hbar\omega\delta N(\omega) = \hbar\omega[N_L(\omega) - N_R(\omega)]$ is a decreasing function with respect to $\omega > 0$ [shown as an inset of Fig. 3(c)], the magnitude of the spectral transfer function at small ω dominates the heat current. The resonant peak of $\mathcal{T}(\omega)$ is located close to $\omega = 0$ at the critical distance where the heat current achieves its maximum. The resonant peak shifts towards larger ω with decreasing distance [as shown in Fig. 3(c) for $\lambda = -0.3$], and this results in a suppressed heat current. Above d_c, the condition for the appearance of resonant peak cannot be satisfied. With increasing distance above d_c, the magnitude of the spectral transfer function decreases, so does the heat current. In the metallic phase, we have $\mathrm{Re}[\chi_L(\omega = 0)] \approx -5$, which means that the critical distance is about 2.6 Å. At such a small gap distance, heat conduction due to electron tunneling happens, and our formalism does not apply [35]. As λ approaches -1, the critical distance increases due to more localized edge states. The maximum heat currents are almost identical in the presence of edge states because they share similar spectral transfer function profiles regardless of the critical gap distances. If the SSH chains experience more dissipation, i.e., larger η, the edge states become less localized, and the critical distance becomes shorter (see Fig. S4 in the Supplemental Material [38]).

In Fig. 4(a), heat current versus λ for $d = 3$ nm is plotted. The heat current for the metallic phase ($\lambda = 0$) is several orders smaller than that for the topologically nontrivial phase. In the trivial insulating phase ($\lambda > 0$), heat current almost vanishes. A sharp jump occurs with the phase transition point $\lambda < 0$, indicating that the presence of edge state can drastically enhance heat current compared to the metallic phase. The spectral transfer functions for different λ are shown in Fig. 4(b). The increase of heat

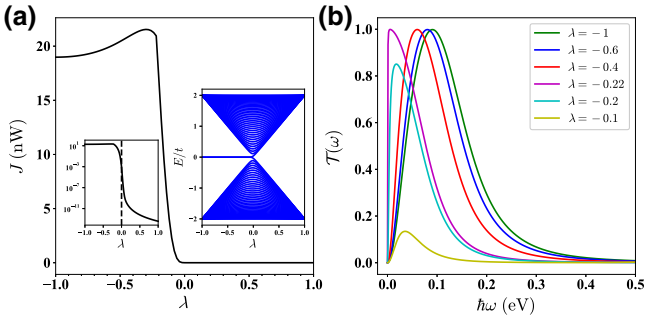

FIG. 4. (a) Heat current by changing λ for $d = 3$ nm. A log-scale plot is shown in the left inset. Energy spectrum of the SSH chain with 160 lattice sites as a function of λ is shown in the right inset. (b) The spectral transfer functions for different λ.

current as λ changes from -1.0 to around -0.22 can be attributed to the shift of the resonant peak of the spectral transfer function towards $\omega = 0$. This is because $d = 3$ nm is the critical distance corresponding to $\lambda = -0.22$. At $\lambda = -0.22$, the resonant peak of the spectral function $\mathcal{T}(\omega)$ is at a frequency close to $\omega = 0$. For $\lambda < -0.22$, the chosen gap separation $d = 3$ nm is smaller than the corresponding critical distance, and the resonant peak locates at a larger frequency. By further increasing λ from -0.22, the SSH chain approaches the metallic phase, and the peak of the spectral transfer function at small angular frequency decreases, and thus heat current reduces. The fact that heat current can be greatly enhanced in the presence of edge states can be exploited to design a near-field thermal switch, provided that the edge states can be tuned.

Summary.– We uncovered the peculiar behaviors of near-field heat transfer in the presence of electronic edge states. Our findings are demonstrated using zigzag SWCNTs and graphene nanotriangles. The underlying mechanism is uncovered through the SSH chains. In the presence of localized zero-energy edge states, heat current is greatly enhanced and shows a nonmonotonic behavior with respect to gap separation. The maximal heat flux between zigzag SWCNTs are shown to be extremely large.

ACKNOWLEDGMENTS

The authors thank Jiebin Peng, Giovanni Vignale, Fuming Xu, and Songbo Zhang for discussions and comments. G.T. and J.S.W. acknowledge the financial support from RSB funded RF scheme (Grant No. R-144-000-402-114). J.R. is supported by the NNSFC (Grant No. 11775159), Shanghai Science and Technology Committee (Grants No. 18ZR1442800, No. 18JC1410900), and the Opening Project of Shanghai Key Laboratory of Special Artificial Microstructure Materials and Technology.

[1] M. Planck and M. Masius, *The Theory of Heat Radiation* (P. Blakiston's Son & Co, New York, 1914).
[2] C. M. Hargreaves, Anomalous radiative transfer between closely-spaced bodies, Phys. Lett. A **30**, 491 (1969).
[3] A. I. Volokitin and B. N. J. Persson, Near-field radiative heat transfer and noncontact friction, Rev. Mod. Phys. **79**, 1291 (2007).
[4] B. Song, A. Fiorino, E. Meyhofer, and P. Reddy, Near-field radiative thermal transport: From theory to experiment, AIP Adv. **5**, 053503 (2015).
[5] D. Polder and M. Van Hove, Theory of radiative heat transfer between closely spaced bodies, Phys. Rev. B **4**, 3303 (1971).
[6] J.-B. Xu, K. Läuger, R. Möller, K. Dransfeld, and I. H. Wilson, Heat transfer between two metallic surfaces at small distances, J. Appl. Phys. **76**, 7209 (1994).
[7] R. S. Ottens, V. Quetschke, S. Wise, A. A. Alemi, R. Lundock, G. Mueller, D. H. Reitze, D. B. Tanner, and B. F. Whiting, Near-field Radiative Heat Transfer between Macroscopic Planar Surfaces, Phys. Rev. Lett. **107**, 014301 (2011).
[8] M. Lim, S. S. Lee, and B. J. Lee, Near-field radiation between doped silicon plates at nanoscale gaps, Phys. Rev. B **91**, 195136 (2015).
[9] A. Kittel, W. MüllerHirsch, J. Parisi, S.-A. Biehs, D. Reddig, and M. Holthaus, Near-Field Heat Transfer in a Scanning Thermal Microscope, Phys. Rev. Lett. **95**, 224301 (2005).
[10] L. Worbes, D. Hellmann, and A. Kittel, Enhanced Near-Field Heat Flow of a Monolayer Dielectric Island, Phys. Rev. Lett. **110**, 134302 (2013).
[11] K. Kloppstech, N. Könne, S.-A. Biehs, A. W. Rodriguez, L. Worbes, D. Hellmann, and A. Kittel, Giant heat transfer in the crossover regime between conduction and radiation, Nat. Commun. **8**, 14475 (2017).
[12] K. Kim, B. Song, V. Fernández-Hurtado, W. Lee, W. Jeong, L. Cui, D. Thompson, J. Feist, M. T. H. Reid, F. J. García-Vidal, J. C. Cuevas, E. Meyhofer, and P. Reddy, Radiative heat transfer in the extreme near field, Nature **528**, 387 (2015).
[13] J. B. Pendry, Radiative exchange of heat between nanostructures, J. Phys.: Condens. Matter **11**, 6621 (1999).
[14] A. I. Volokitin and B. N. J. Persson, Resonant photon tunneling enhancement of the radiative heat transfer, Phys. Rev. B **69**, 045417 (2004).
[15] S. Shen, A. Narayanaswamy, and G. Chen, Surface phonon polaritons mediated energy transfer between nanoscale gaps, Nano Lett. **9**, 2909 (2009).
[16] K. Ito, T. Matsui, and H. Iizuka, Thermal emission control by evanescent wave coupling between guided mode of resonant grating and surface phonon polariton on silicon carbide plate, Appl. Phys. Lett. **104**, 10 (2014).
[17] J. P. Mulet, K. Joulain, R. Carminati, and J. J. Greffet, Enhanced radiative heat transfer at nanometric distances, Microscale Thermophys. Eng. **6**, 209 (2002).
[18] H. Iizuka and S. Fan, Analytical treatment of near-field electromagnetic heat transfer at the nanoscale, Phys. Rev. B **92**, 144307 (2015).
[19] S. V. Boriskina, J. K. Tong, Y. Huang, J. Zhou, V. Chiloyan, and G. Chen, Enhancement and tunability of near-field radiative heat transfer mediated by surface plasmon polaritons in thin plasmonic films, Photonics **2**, 659 (2015).
[20] J.-P. Mulet, K. Joulain, R. Carminati, and J.-J. Greffet, Nanoscale radiative heat transfer between a small particle and a plane surface, Appl. Phys. Lett. **78**, 2931 (2001).
[21] O. Ilic, M. Jablan, J. D. Joannopoulos, I. Celanovic, H. Buljan, and M. Soljacic, Near-field thermal radiation transfer controlled by plasmons in graphene, Phys. Rev. B **85**, 155422 (2012).
[22] F. V. Ramirez, S. Shen, and A. J. H. McGaughey, Near-field radiative heat transfer in graphene plasmonic nanodisk dimers, Phys. Rev. B **96**, 165427 (2017).
[23] R. Yu, A. Manjavacas, and F. J. García de Abajo, Ultrafast radiative heat transfer, Nat. Commun. **8**, 2 (2017).
[24] Y. Zhang, H.-L. Yi, and H.-P. Tan, Near-field radiative heat transfer between black phosphorus sheets via anisotropic surface plasmon polaritons, ACS Photonics **5**, 3739 (2018).

[25] E. Rousseau, Ma. Laroche, and J.-J. Greffet, Radiative heat transfer at nanoscale mediated by surface plasmons for highly doped silicon, Appl. Phys. Lett. **95**, 231913 (2009).
[26] V. Fernández-Hurtado, F. J. García-Vidal, S. Fan, and J. C. Cuevas, Enhancing Near-Field Radiative Heat Transfer with Si-based Metasurfaces, Phys. Rev. Lett. **118**, 203901 (2017).
[27] I. Latella, R. Messina, J. M. Rubi, and P. Ben-Abdallah, Radiative Heat Shuttling, Phys. Rev. Lett. **121**, 023903 (2018).
[28] S.-A. Biehs, M. Tschikin, and P. Ben-Abdallah, Hyperbolic Metamaterials as an Analog of a Blackbody in the Near Field, Phys. Rev. Lett. **109**, 104301 (2012).
[29] S.-A. Biehs, M. Tschikin, R. Messina, and P. Ben-Abdallah, Super-Planckian near-field thermal emission with phonon-polaritonic hyperbolic metamaterials, Appl. Phys. Lett. **102**, 131106 (2013).
[30] O. D. Miller, S. G. Johnson, and A. W. Rodriguez, Effectiveness of Thin Films in Lieu of Hyperbolic Metamaterials in Near Field, Phys. Rev. Lett. **112**, 157402 (2014).
[31] A. Pérez-Madrid, J. M. Rubí, and L. C. Lapas, Heat transfer between nanoparticles: Thermal conductance for near-field interactions, Phys. Rev. B **77**, 155417 (2008).
[32] D. Becerril and C. Noguez, Near-field energy transfer between nanoparticles modulated by coupled multipolar modes, Phys. Rev. B **99**, 045418 (2019).
[33] G. D. Mahan, Tunneling of heat between metals, Phys. Rev. B **95**, 115427 (2017).
[34] J.-S. Wang and J. Peng, Capacitor physics in ultra-near-field heat transfer, Europhys. Lett. **118**, 24001 (2017).
[35] Z.-Q. Zhang, J.-T. Lü, and J.-S. Wang, Energy transfer between two vacuum-gapped metal plates: Coulomb fluctuations and electron tunneling, Phys. Rev. B **97**, 195450 (2018).
[36] J.-S. Wang, Z.-Q. Zhang, and J.-T. Lü, Coulomb-force-mediated heat transfer in the near field: Geometric effect, Phys. Rev. E **98**, 012118 (2018).
[37] G. Tang and J.-S. Wang, Heat transfer statistics in extreme-near-field radiation, Phys. Rev. B **98**, 125401 (2018).
[38] See Supplemental Material at http://link.aps.org/supplemental/10.1103/PhysRevApplied.11.031004 for the argument of the nonretardation limit, conditions for reaching maximal heat current, a comparison between zigzag and armchair SWCNTs, heat-current contribution from each site for nanographene triangles, and the influence of damping parameter, temperature, and chemical potential on the heat transfer.
[39] R. Messina, S.-A. Biehs, T. Ziehm, A. Kittel, and P. Ben-Abdallah, Heat transfer between two metals through subnanometric vacuum gaps, arXiv:1810.02628.
[40] M. Settnes, J. R. M. Saavedra, K. S. Thygesen, A.-P. Jauho, F. J. García de Abajo, and N. A. Mortensen, Strong plasmon-phonon splitting and hybridization in 2D materials revealed through a self-energy approach, ACS Photonics **4**, 2908 (2017).
[41] S. Thongrattanasiri, A. Manjavacas, and F. J. García de Abajo, Quantum finite-size effects in graphene plasmons, ACS Nano **6**, 1766 (2012).
[42] M. Fujita, K. Wakabayashi, K. Nakada, and K. Kusakabe, Peculiar localized state at zigzag graphite edge, J. Phys. Soc. Jpn. **65**, 1920 (1996).
[43] K. Nakada, M. Fujita, G. Dresselhaus, and M. S. Dresselhaus, Edge state in graphene ribbons: Nanometer size effect and edge shape dependence, Phys. Rev. B **54**, 17954 (1996).
[44] Ken-ichi Sasaki, Kentaro Sato, Riichiro Saito, Jie Jiang, Seiichiro Onari, and Yukio Tanaka, Local density of states at zigzag edges of carbon nanotubes and graphene, Phys. Rev. B **75**, 235430 (2007).
[45] C. H. Lewenkopf and E. R. Mucciolo, The recursive Green's function method for graphene, J. Comput. Electron **12**, 203 (2013).
[46] B. Liu, F. Wu, H. Gui, M. Zheng, and C. Zhou, Chirality-controlled synthesis and applications of single-wall carbon nanotubes, ACS Nano **11**, 31 (2017).
[47] Q. Zhao, Z. Xu, Y. Hu, F. Ding, and J. Zhang, Chemical vapor deposition synthesis of near-zigzag single-walled carbon nanotubes with stable tube-catalyst interface, Sci. Adv. **2**, 1501729 (2016).
[48] M. Settnes, S. R. Power, J. Lin, D. H. Petersen, and A.-P. Jauho, Patched Green's function techniques for two-dimensional systems: Electronic behavior of bubbles and perforations in graphene, Phys. Rev. B **91**, 125408 (2015).
[49] W. P. Su, J. R. Schrieffer, and A. J. Heeger, Solitons in Polyacetylene, Phys. Rev. Lett. **42**, 1698 (1979).
[50] Y. Peng, Y. Bao, and F. vonOppen, Boundary Green functions of topological insulators and superconductors, Phys. Rev. B **95**, 235143 (2017).